Journal of Power Sources 188 (2009) 268–273

Contents lists available at ScienceDirect

Journal of Power Sources

journal homepage: www.elsevier.com/locate/jpowsour

Microstructure and electrochemical performance of thin film anodes for lithium ion batteries in immiscible Al–Sn system

Renzong Hu [a], Meiqin Zeng [a], Chi Ying Vanessa Li [b], Min Zhu [a,*]

[a] School of Materials Science and Engineering, South China University of Technology, Guangzhou 510640, PR China
[b] School of Materials Science and Engineering, University of New South Wales, Sydney, NSW 2052, Australia

ARTICLE INFO

Article history:
Received 16 August 2008
Received in revised form 11 November 2008
Accepted 17 November 2008
Available online 24 November 2008

Keywords:
Immiscible alloy system
Al–Sn alloy
Electron-beam deposition
Anode
Lithium ion batteries

ABSTRACT

The immiscible Al–Sn alloy thin films prepared by electron-beam deposition were first investigated as possible negative electrodes for lithium ion batteries. In the complex structure of the Al–Sn thin films, tiny Sn particles dispersed homogeneously in the Al active matrix. Their electrochemical characteristics were tested in comparison with the pure Al and Sn films. Cyclic voltammetry results indicated that the Li^+-transport rates in these Al–Sn alloy films were significantly enhanced. Charge–discharge tests showed that the Al–Sn alloy film anodes had good cycle performance. The electrode with high Al content (Al–33 wt%Sn) delivered a high initial discharge capacity of 752 mAh g^{-1} while the electrode with high Sn content (Al–64 wt%Sn) had better cycleability with a stable specific capacity of about 300 mAh g^{-1} under 0.8 C rate. The good performance of these immiscible Al–Sn alloy film anodes was attributed to their unique microstructure. The mechanism of lithiation and delithiation reaction had been proposed based on cyclic voltammograms and impedance response of the Al–Sn alloy thin film electrodes. Our preliminary results demonstrate that the Al–Sn immiscible alloy is a potential candidate negative material for Li-ion battery.

1. Introduction

Tremendous effort has now been devoted to improve the performance of lithium ion batteries by developing new electrode materials that possess enhanced energy content. Since the metal–Sn can store more lithium and deliver higher capacity ($Li_{4.4}Sn$: 994 mAh g^{-1}) than graphite (LiC_6: 372 mAh g^{-1}), thus it is possible that Sn-based alloys could replace carbonaceous anodes. However, pure Sn electrodes suffer from severe mechanical disintegration caused by the drastic volume change during the lithium insertion and extraction process, resulting in capacity degradation which greatly limits the application [1,2].

In order to enhance cycling performance, Winter and his coworkers [3–6] proposed the use of intermetallic compounds consist of "active/active components" as optimized electrodes with controlled volume stresses. Using $SnSb_x$ phase as an example to illustrate the "active/active components" idea, Sn and Sb being the active components, they would each react with lithium at different potentials. At anytime, the non-reacting component (either Sn or Sb) can "buffer" the volume change of the reacting phase (corresponds to Sb or Sn) during its alloying with lithium, consequently leads to a good operational stability of the electrode. It is well known that the biggest drawback in the inactive/active compounds such as Cu_6Sn_5 [7–9] is the capacity loss in the system due to the presence of inactive components (Cu). This is overcome by the $SnSb_x$ system as the capacity loss is compensated by both active components as host materials. Therefore, these all-active composites present good capacity retention and high capacity performance.

Al–Sn alloy, as an all-active composite, where the Al component reacts reversibly with lithium and forms LiAl and Li_9Al_4 phases, delivering a specific capacity of 993 and 2234 mAh g^{-1}, respectively [10]. Considering the extremely high capacity that could be achieved, Al–Sn alloy truly stands as a potential anode material for lithium ion batteries. However, to our best knowledge, the use of this alloy in lithium ion battery is very limited [11]. Al–Sn is an immiscible alloy system, which means that there is no intermetallic and solid solution phase in this system. Thus, this unique active/active composite would show different lithiation/delithiation mechanism comparing with those systems containing intermetallic compounds (e.g. Cu_6Sn_5, SnSb, etc.).

This paper reports the electrochemical behavior of the Al–Sn thin films prepared by electron-beam deposition, as anodes for lithium ion batteries. A novel strategy is used to prepare Al–Sn alloy thin films with complex structures in which microcrystalline Sn particles dispersed homogeneously in the Al active matrix. Since the diffusion coefficient of Li^+ in Sn is much higher than that in

* Corresponding author. Tel.: +86 20 87113924; fax: +86 20 87111317.
E-mail address: memzhu@scut.edu.cn (M. Zhu).

0378-7753/$ – see front matter © 2008 Elsevier B.V. All rights reserved.
doi:10.1016/j.jpowsour.2008.11.059

Table 1
Deposition conditions and parameters for the Al–Sn thin film electrodes.

Sample	Vacuum	Voltage	Current, deposition time
Al–33 wt%Sn	3.1×10^{-3} Pa	7 kV	Step 1—Sn: 80 mA × 30 min Step 2 (co-deposition)—Al, Sn: 80 mA × 15 min
Al–64 wt%Sn	2.9×10^{-3} Pa	7 kV	Step 1—Sn: 80 mA × 60 min Step 2 (co-deposition)—Al, Sn: 80 mA × 15 min

LiAl phase [10,12], it is expected that such structured Al–Sn film can enhance Li^+ transportation dramatically. Due to different lithiation potentials of Sn and Al, the reactions of each phase are in sequence; thus the expansion of the reacting phase can be buffered by the unreacted phase, improving the cycle life of the Al–Sn film electrode.

2. Experimental

2.1. Preparation of Al–Sn alloy thin film electrodes

The Al–Sn thin films were deposited on Cu foil substrates by an electron-beam (e-beam) evaporator with two source units. In the deposition, a Sn layer was deposited on Cu foil first, and then Al–Sn composite was co-deposited by evaporating Sn and Al target spontaneously on the pre-deposited Sn layer. The ratio of Al to Sn in thin films was controlled by adjusting the evaporation rate from each single source. Two composition types of Al–Sn alloy films were prepared: Al–33 wt%Sn and Al–64 wt%Sn. Pure Sn and Al films were also prepared by e-beam evaporator for comparison. The thickness of the films was controlled to be approximately the same by the input power and evaporation time (see Table 1), and was measured using the quartz crystal oscillation attached to the evaporator. The weight of active material in Al–33 wt%Sn and Al–64 wt%Sn samples was 0.64 and 0.50 mg cm^{-2}, respectively.

2.2. Characterization

The microstructure of the thin film electrodes was characterized by X-ray diffraction (XRD) Philips X'pert MPD with Cu Kα radiation and scanning electron microscopy (SEM) LEO 1530 VP FE-SEM. The compositions of the samples were analyzed by an INCA300 EDS attached to SEM. DSC measurement was performed for the as-deposited Al–Sn films using a Pyris Diamond DSC (PerkinElmer, USA) at a heating rate of 10 °C min^{-1}.

2.3. Electrochemical measurement

Electrochemical responses of the deposited film anodes were investigated directly using CR2016 coin-type half-cells assembled in an argon-filled glove box. The cell was comprised of lithium metal as counter and reference electrodes, and the as-deposited film (10 mm × 10 mm) as negative electrodes; the electrodes were separated by separators in the cell. The electrolyte was $LiPF_6$ (1 M) in a mixture of EC + DEC + EMC (1:1:1, v/v/v). Cycling tests were carried out at room temperature using current density of 0.1, 0.2 and 0.4 mA cm^{-2}, respectively, in the voltage range of 0.05–1.25 V, controlled by the Arbin BT-2000 battery test system. Cyclic voltammograms (CV) were measured by AutoLab Electrochemical System (ECO Chemie) in the range of 0.0–1.5 V at scanning rates of 0.1, 0.2, 0.3, 0.4, 0.5 and 0.6 mV s^{-1}, respectively. The impedance spectroscopy analysis was carried out by applying a 5 mV amplitude signal in the 1 MHz to 0.1 Hz frequency range using a frequency response analyzer coupled with Auto Lab Electrochemical System.

3. Results and discussion

3.1. Structure of the as-deposited Al–Sn alloy thin films

Fig. 1 shows the SEM images of as-deposited Al–Sn alloy thin film surface. With respect to the Al–33 wt%Sn thin film as shown in Fig. 1a, the Al matrix was comprised of micro-spherical particles, whereas, most of the Sn particles of about 2 μm in size are homogeneously dispersed in it and the Sn particles on surface are penetrated through the boundaries and cavities of Al matrix. The morphology of Al–63 wt%Sn sample is quite different to that of the Al–33 wt%Sn sample, as shown in Fig. 1b, its Al matrix is less dense and the size of Sn particles is smaller than those of the Al–33 wt%Sn film. These morphology differences between the samples may be due to the difference in the composition. The insertions in Fig. 1a and b are the cross-section images of the as-deposited Al–Sn thin films and they clearly show that the films are constructed by a Sn layer (the bright layer on the Cu foil substrate) and followed by an Al–Sn composite layer. As shown in Fig. 2, the two samples have quite different thermal characteristic due to the difference in mor-

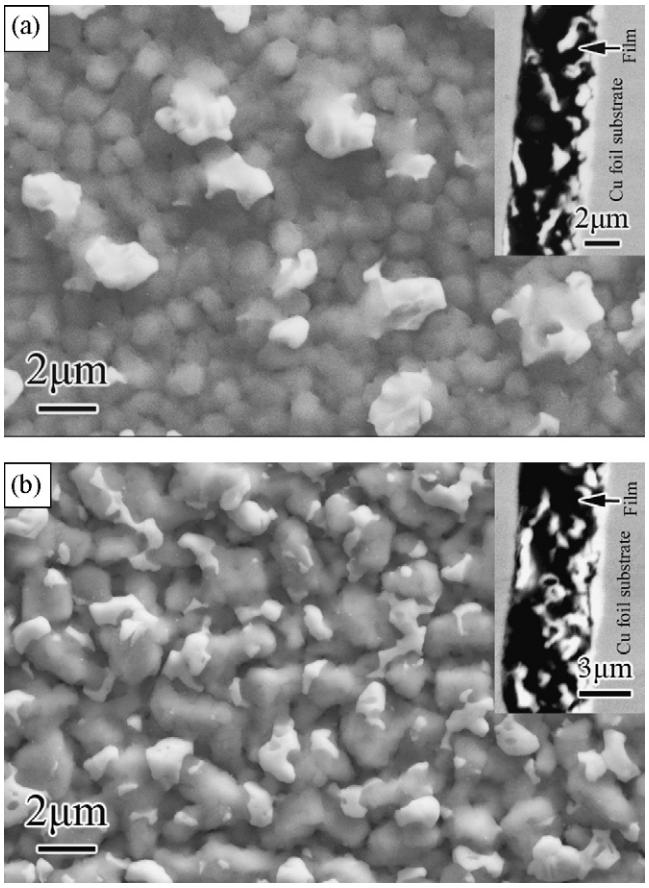

Fig. 1. SEM images of (a) Al–33 wt%Sn and (b) Al–64 wt%Sn thin films prepared by e-beam deposition, the insertions are the cross-section images. The bright particles are Sn phase and the dark area is the Al matrix.

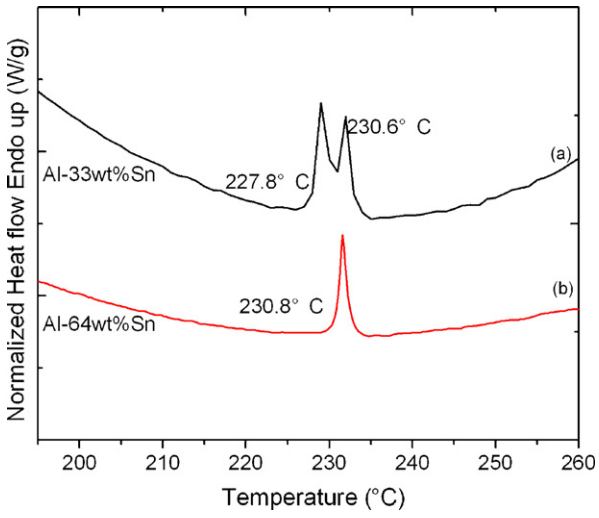

Fig. 2. DSC heating curves of as-deposited (a) Al–33 wt%Sn and (b) Al–64 wt%Sn thin films. The thin films were heated at the rate of 10 °C min^{-1} in nitrogen.

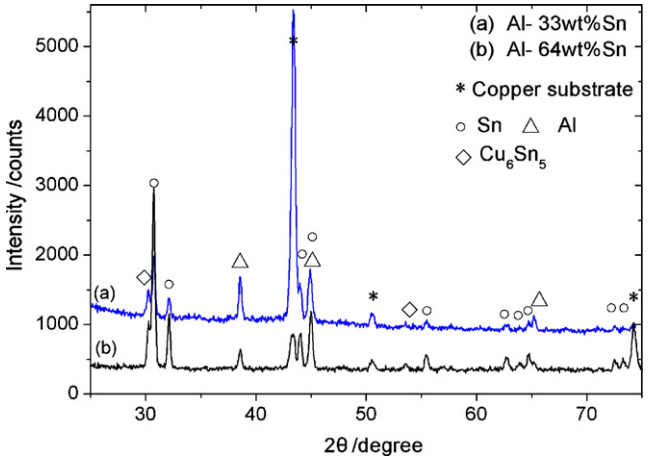

Fig. 3. XRD patterns of the as-deposited thin film electrodes: (a) Al–33 wt%Sn and (b) Al–64 wt%Sn.

phology and composition of thin films. Two endothermic peaks around 227.8 and 230.6 °C, respectively are observed on the DSC heating curve of Al–33 wt%Sn thin film, which are attributed to the eutectic reaction of Sn–Al alloy and melting of Sn. However, there is only one endothermic peak at 230.8 °C induced by the melting of Sn on the Al–64 wt%Sn thin film. All these temperatures are a bit depressed possibly owing to the tiny Sn grains and microcrystals in the e-beam deposited Sn–Al alloy films.

For Al–Sn films deposition, due to low melting point of Sn (231.9 °C), the evaporation and deposition rate of Sn was high. Therefore, coarse poly-crystal grains of Sn were formed in the pre-deposited Sn layer. The co-deposited layer was mainly comprised of Al element (as shown in Fig. 1) because the vapor pressure of Al is much higher than that of Sn under the same condition. The pre-deposited Sn layer would be melted because extra heat was brought to the film when the Al particles were deposited as the melting point of Al (660.5 °C) is much higher than that of Sn. Meanwhile, as Sn was immiscible with Al element, no intermetallic or solid solution phase was formed. In this case, the melted Sn penetrated into the grain boundaries and/or microvoids in the Al matrix by both gravitation effect and surface tension. Thus, a unique crystallinity and distribution of Al–Sn alloy film was formed as shown in SEM image in Fig. 1.

Fig. 3 shows the X-ray diffraction patterns of the as-deposited Al–Sn alloy thin films. Besides those reflections from the Cu substrate and some small peaks corresponding to the reflection of Cu_6Sn_5 intermetallic phases in Cu–Sn system, which might be formed between the interface of Sn layer and Cu foil substrate during the process of deposition, the diffraction peaks of Al–33 wt%Sn (Fig. 3a) and Al–64 wt%Sn (Fig. 3b) are attributed to Sn and Al phases. There is no apparent shift of Al and Sn peaks meaning that there is no obvious dissolution of Sn to Al or vice versa.

3.2. Electrochemical properties of the Al–Sn alloy thin film anodes

3.2.1. Cyclic voltammograms

Fig. 4 shows the curves of the second scan of cyclic voltammetry (CV) measurement for pure Al, pure Sn, Al–33 wt%Sn and Al–64 wt%Sn thin film electrodes made between 0.0 and 1.5 V at a scanning rate of 0.5 mV s^{-1}. The electrochemical activities of these immiscible Al–Sn alloy films are evidenced by the CVs, where well-resolved reversible peaks are observed at near 0.10, 0.20, 0.38, 0.50 and 0.70 V upon discharge and broad peaks are observed at 0.50 and 0.80 V upon charge for both of the Al–33 wt%Sn and Al–64 wt%Sn samples. Comparing with peaks in CVs of pure Al and pure Sn electrodes, the reduction peaks of Al–Sn alloys at 0.10 and 0.20 V are attributed to lithium alloying with Al while the peaks of 0.38, 0.50 and 0.70 V are attributed to lithium reacting with Sn. However, it is found that the reduction peaks in these alloy electrodes shift a bit to the right as the composition of Sn increases, which is possibly because that the lithiation potential of Sn element is higher than that of Al as shown in Fig. 4. There, the peaks of them are overlapped when parts of Al and Sn are active synchronously. In the case of pure Sn electrode, an irreversible reduction peak appears at 1.40 V vs. Li/Li$^+$, which corresponds to the formation of solid electrolyte interface (SEI) film on the surface of Sn electrode. However, no peak associated to SEI formation was observed on the pure Al and Al–Sn alloy film electrodes, indicating that little irreversible consumption of materials, e.g. lithium and electrolyte, would happen in the Al–Sn alloy electrodes.

3.2.2. Diffusion coefficient

The variation in peak shape of the CV curves with scan rate (ν) reflects the kinetics of lithium intercalation/deintercalation at the electrode/electrolyte interface and/or the rate of lithium diffusion inside the film electrode. A series of voltammetric curves are recorded with Al–33 wt%Sn electrode as function of scan rate ν in the range from 0.1 to 0.5 mV s^{-1}. As shown in Fig. 5a, an increase in

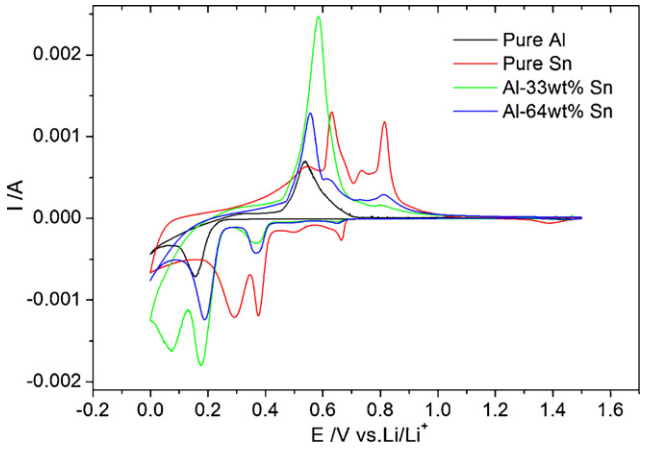

Fig. 4. Cyclic voltammograms of as-deposited pure Sn, pure Al, Al–33 wt%Sn and Al–64 wt%Sn thin film electrodes measured with a scanning rate of 0.5 mV s^{-1} during the second cycle.

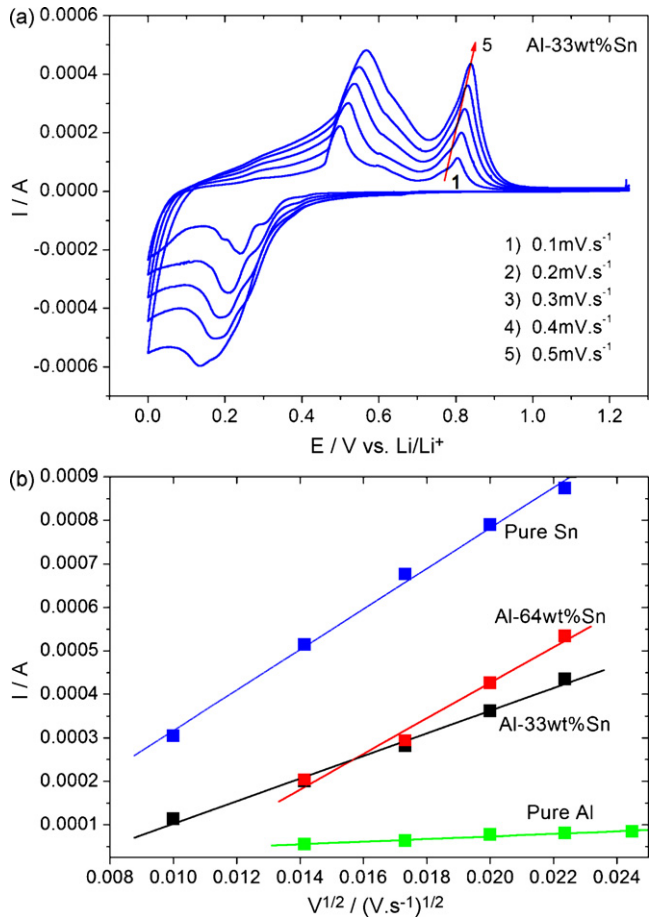

Fig. 5. (a) Cyclic voltammograms of Al–33 wt%Sn thin film electrode measured at the range of 0–1.25 V with different scanning rates and (b) the relationship between I_p and $\nu^{1/2}$, in which those of pure Sn, pure Al and Al–64 wt%Sn samples were also presented.

ν is correlated with a progressive shift of the anodic peaks to higher potential as well as an increase in peak height. It also has been found that, as shown in Fig. 5b, the peak current (I_p, the peak near 0.8 V) is approximately proportional to the root of the scan rate ($\nu^{1/2}$) and can be expressed by the following equation [13,14], which indicates that the reaction kinetics are controlled by the diffusion step:

$$I_p = 2.69 \times 10^5 A n^{3/2} C_0 D^{1/2} \nu^{1/2}$$

where n is the number of electrons per molecules during the intercalation (Li^+, $n = 1$), A is the surface area of the electrode (1 cm^2 in this work), C_0 is the initial concentration of lithium ions (1 mol L^{-1} in electrolyte). D is the diffusion coefficient of Li^+. According to Fig. 5b, the D_{Li^+} calculated out is 0.9×10^{-8} cm^2 s^{-1} for the Al–33 wt%Sn thin film electrode. By the same way, D_{Li^+} in the Al–64 wt%Sn, pure Sn and pure Al thin film anodes are also determined and listed in Table 2. The above results indicate that the transportation rates of Li^+ in those immiscible Al–Sn alloy films are similar to that of Sn film but are about two orders higher than

Table 2
Diffusion coefficient of Li^+ in pure Al, pure Sn, Al–33 wt%Sn and Al–64 wt%Sn thin film electrodes.

Thin film sample	Diffusion coefficient, D_{Li^+} (cm^2 s^{-1})
Pure Al	1.2×10^{-10}
Pure Sn	3.0×10^{-8}
Al–33 wt%Sn	0.9×10^{-8}
Al–64 wt%Sn	2.3×10^{-8}

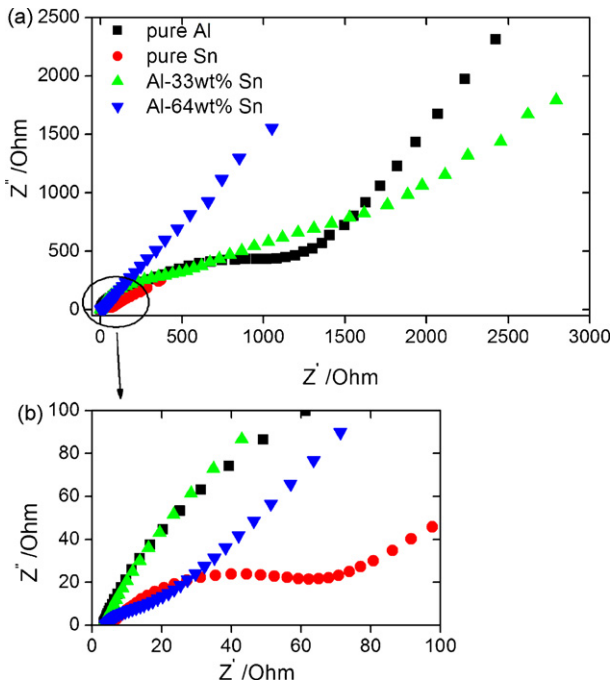

Fig. 6. Impedance spectra of pure Al, pure Sn, Al–33 wt%Sn and Al–64 wt%Sn thin film electrodes before charge–discharge cycling of the cells. (a) Full scale and (b) enlarged view of the high frequency domain of the impedance spectra. Amplitude: 5 mV, frequency range: 1 MHz to 0.1 Hz.

that in the pure Al film. This is attributed to the unique structure and morphology of the e-beam deposited Al–Sn films as the microcrystalline Sn particles penetrated through the Al matrix (see Fig. 1) serve as the diffusion channels for Li^+ in the Al–Sn thin film anodes. Thus the Li^+-transportation rate in Al–Sn alloy electrodes is close to Sn, which also indicates that the Al–Sn thin film anodes should have better C-rate capability and charge/discharge cycle performance.

3.2.3. AC impedance

The impedance spectra of the cells with the above four thin film electrodes were measured before charge–discharge cycle and given in Fig. 6. The semicircle appearing at high frequencies is related to resistance of the electrode surface. As shown in Fig. 5a, for pure Al electrode, the large semicircle indicates high resistance of surface film on the pure Al electrode. However, the semicircles of both Al–33 wt%Sn and Al–64 wt%Sn electrodes are distinctly decreased. This result indicates the lower resistance of the surface film and charge transfer reaction, namely better electronic connection for the Al–Sn film anodes. From the enlargement of the high frequency region shown in Fig. 6b, it can be seen that the semicircle of Al–33 wt%Sn electrode is larger than that of the pure Sn electrode. However, the semicircle of the Al–64 wt%Sn electrode is much smaller, which indicated that its resistance of surface film is much lower. Based on the analysis mentioned above, it can be concluded that the immiscible alloy system Al–Sn film electrode, especially the Sn rich electrode, e.g. Al–64 wt%Sn sample, presents very low resistance of surface film and high diffusion rate of Li^+ in the electrode, which is consistent with the cyclic voltammetry results shown in Fig. 5. Thus, the Al–Sn alloy film electrode would show better electrochemical performances than those of the pure Al.

3.2.4. Charge/discharge curves and cycle performance

Fig. 7a and b shows the voltage profiles of the initial cycles of the Al–33 wt%Sn and Al–64 wt%Sn thin film electrodes, respectively, in a lithium cell. For comparison, the voltage profiles of pure Al and

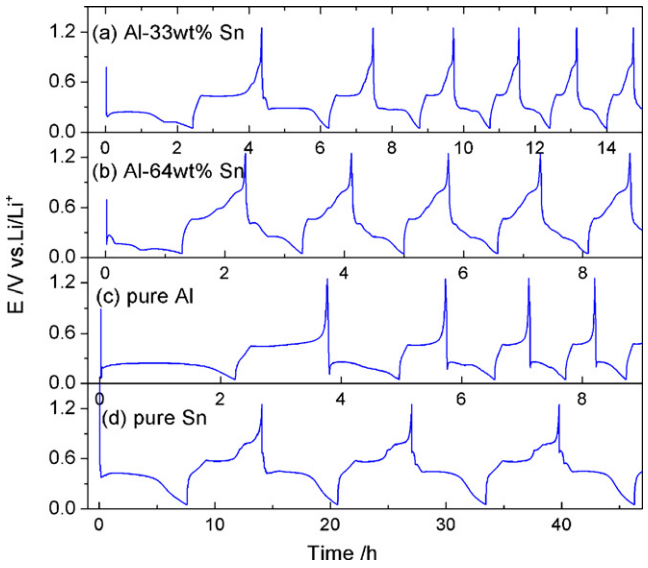

Fig. 7. Initial voltage profiles of electrode: (a) Al–33 wt%Sn, (b) Al–64 wt%Sn, (c) pure Al and (d) pure Sn. Voltage range: 0.05–1.25 V vs. Li/Li$^+$. Current density: 0.2 mA cm^{-2}.

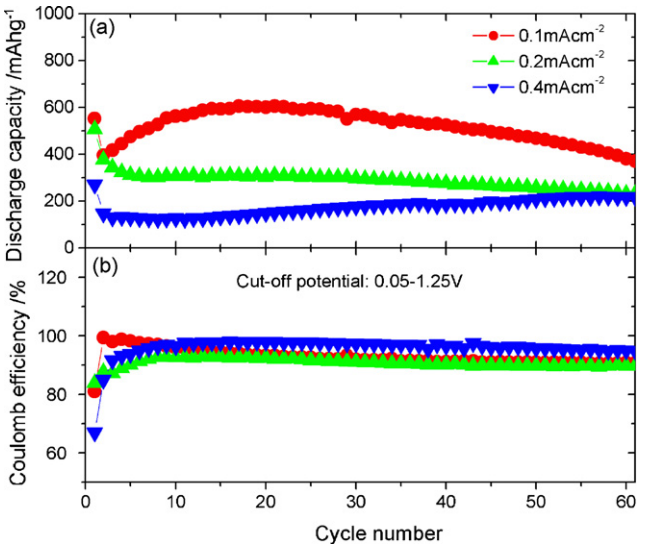

Fig. 9. Cycle performance of Al–64 wt%Sn thin film electrode made under various current densities: (a) discharge capacities and (b) efficiencies. Voltage range: 0.05–1.25 V vs. Li/Li$^+$. Current density: 0.1, 0.2 and 0.4 mA cm^{-2} (ca. 0.4, 0.8 and 1.2 C).

pure Sn samples were also given in this figure. It is evident from Fig. 7a and b that several processes take place during the electrochemical discharge and charge reactions, which associated with different lithium alloying (discharge)/lithium de-alloying (charge) stages. It is assumed that, in comparison with the voltage profiles of pure Al (Fig. 7c) and pure Sn (Fig. 7d) samples, the multi-plateau behavior of these immiscible alloy electrodes is attributed to the successive electrochemical reactions of Sn phase and Al phase with Li, which is consistent with the results of CVs as shown in Fig. 4. The discharge–charge curves in cycles are similar, which presents good reversibility and indicates that the same lithium-active phase of the film provides a stable reaction with Li during cycling. However, the phases formed on each reaction step have been not identified and require further investigation by the method such as in situ X-ray diffraction.

Fig. 8 shows the cycle performances of the pure Al, pure Sn, Al–33 wt%Sn and Al–64 wt%Sn thin film electrodes under the current density of 0.2 mA cm^{-2} (ca. 0.8 C) and potential range from 0.05 to 1.25 V. Although the pure Al and pure Sn electrodes deliver very high initial discharge capacities, the capacity retentions of them are very poor. With respect to the Al–Sn alloy thin film electrodes, the

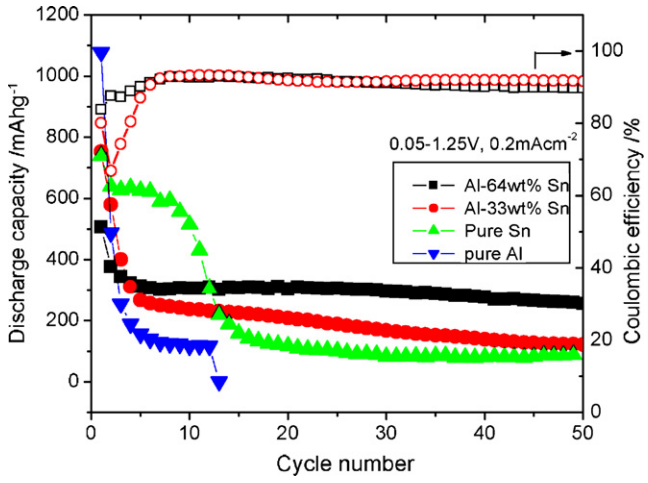

Fig. 8. Cycle performances of pure Al, pure Sn, Al–33 wt%Sn and Al–64 wt%Sn thin film electrodes. Voltage range: 0.05–1.25 V vs. Li/Li$^+$. Current density: 0.2 mA cm^{-2}.

Al rich electrode, Al–33 wt%Sn sample delivers an initial discharge capacity of 752 mAh g^{-1}, which is lower than that of the pure Al electrode. However, it shows much better capacity retention than the pure Al electrode. For Sn rich film electrode (Al–64 wt%Sn), on the other hand, its initial discharge capacity is less than that of the pure Sn electrode. However, the Al–64 wt%Sn film electrode shows the best cycle performance in comparison with the other three electrodes. The initial discharge capacity and columbic efficiency of Al–64 wt%Sn electrode are 506 mAh g^{-1} and 83%, respectively. After dramatically decreasing at the first several cycles possibly due to the "rearrangement" of the thin film structure [12], the electrode delivers a specific capacity of 300 mAh g^{-1} and this value remains stable over more than 50 cycles.

Fig. 9 compares the cycle performance of Al–64 wt%Sn electrode measured at different current densities. It shows that a small current density can evidently enhance electrode capacity. It is interesting to note that, as shown in Fig. 9a, the discharge capacity increases from the second cycle and reaches the maximum discharge capacity of 606 mAh g^{-1} at the 21st cycle when the Al–64 wt%Sn electrode was cycled at 0.1 mA cm^{-2}. Thus, the active materials in the Al–64 wt%Sn electrode took 20 cycles to activate. Moreover, this can be due to the increase of surface area accompanying with the volume change during cycling, which is expected to increase the reactivity of the electrode against Li$^+$. When the electrode was cycled at a higher current density of 0.4 mA cm^{-2}, the discharge capacity is relatively low, which is less than 200 mAh g^{-1} for the first 40 cycles. Maybe it is because that the lithiation reaction in the film electrode was lagging behind the potential drop at higher discharge current density due to the low Li$^+$ diffusion rate in Al matrix, which causes lower potential of the discharge curve at the first cycle than the others in the Al–Sn alloy electrodes as shown in Fig. 6a and b. These results in most of the active materials, i.e. Al and Sn, remaining where electrode potential reaches the cutoff voltage before all-active phases react and thus delivers lower capacity. However, the Li$^+$ diffusion might be enhanced in the Al–Sn alloy film after prolong lithium insertion/extraction cycles, as observed in the increase in capacity after 30 cycles (Fig. 9a).

The columbic efficiency of Al–64 wt%Sn is illustrated in Fig. 9b. It takes 10 cycles for the electrode to reach full efficiency when discharged at 0.2 and 0.4 mA cm^{-2}, but it only takes 1 cycle when discharge at 0.1 mA cm^{-2}. The initial columbic efficiency is 70%, thus 30% is irreversible which is quite likely to be caused

by a series of irreversible process, which include: (i) electrolyte decomposition with the formation of SEI film on electrode surface; (ii) trapping initial lithium in structure defect sites; (iii) reduction of residual impurities (e.g. SnO_2, Al_2O_3, etc.); (iv) the rearrangement of electrode structure [15]. However, it needs further investigation to identify the cause of the irreversible capacity and reduce to an acceptable level in this immiscible Al–Sn alloy electrode.

Based on the above-mentioned experimental results, the lithiation behaviors of the immiscible alloy Al–Sn thin film electrodes are proposed as follow. In the initial cycles, it is just the Al and the Sn in the top composite layer in the electrode reacting with Li due to the low Li^+ diffusion rate in the Al matrix. This hypothesis can be confirmed by the fact that the first discharge profiles of Al–Sn alloy samples (see Fig. 7a and b) are particularly similar to that of the typical galvanostatic plot of the pure Al electrode (see Fig. 7c), which indicates that Al is the main reactant phase. Meanwhile, the initial discharge capacity of Al–33 wt%Sn sample (752 mAh g^{-1}) is higher than that of the Al–64 wt%Sn sample (506 mAh g^{-1}), which can be ascribed to the capacity delivered by different Al component in the two samples. As the cycle number increases, the Sn particles that penetrated through the Al matrix completely reacted with Li and may enhance the diffusion rate of Li^+ ion. And thus the reacted Sn phases act as the diffusion channels for the Li^+ to insert into the inner Sn layer. As the Li^+ diffusion rate in Sn is much higher than that in Al phase (see Table 2), the lithiating/delithiating rate to Al/from LiAl lagged behind the potential change. Therefore, part of the Al in the film electrode would not react with Li during discharge while part of the LiAl would not delithiate during charge. These remaining Al and LiAl phases would act as the buffer and stabilize the reacting phases, thus, improving the stability and cycle performance of the thin film electrodes. The exact lithiation and delithiation behaviors in the thin film electrodes of the immiscible Al–Sn alloy system would require further investigation. Moreover, the initial discharge capacities of Al–33 wt%Sn and Al–64 wt%Sn under current density of 0.2 mA cm^{-2} (752 and 506 mAh g^{-1}, respectively) are much lower than their theoretical capacity of about 994 mAh g^{-1} given by $[0.67 \times 993_{LiAl} + 0.33 \times 994_{Li_{4.4}Sn}]$ and $[0.36 \times 993_{LiAl} + 0.64 \times 994_{Li_{4.4}Sn}]$, respectively. It may be due to that part of the active phases (i.e. Al and Sn) did not reacted with Li and remained under the applied charging/discharging current density, and thus decreased the energy density of the film electrode reported here. It has also been found that the profile of the discharge curve and its corresponding discharge capacity of the Al–Sn alloy thin film electrodes obviously depended on the applied current density but requires further identification.

4. Conclusions

For the first time, immiscible Al–Sn composite thin films with high and low Sn content have been prepared by electron-beam deposition to fabricate as an anode in lithium ion batteries. The Al–Sn thin film is of two layers, i.e. a Sn layer covered by an Al–Sn composite layer in which tiny Sn particles dispersed on Al matrix. This unique microstructure leads to the good performance of this immiscible Al–Sn alloy thin film anodes. The electrode with high Al content (Al–33 wt%Sn) delivers a relatively high initial discharge capacity of 752 mAh g^{-1}, while the electrode with high Sn content (Al–64 wt%Sn) can undergo longer cycle life with a stable specific capacity of about 300 mAh g^{-1}. Cyclic voltammetry results indicated that the reaction kinetics were controlled by a lithium diffusion step and the transportation rate of Li^+ in Al–Sn alloy films is significantly enhanced when compared to that of pure Al film electrode.

Acknowledgements

This work was supported by Ministry of Education under project no. IRT0551 and Guangdong Provincial Natural Science Foundation under the Team Project.

References

[1] M. Winter, J.O. Besenhard, Electrochim. Acta 45 (1999) 31.
[2] I.A. Courtney, J.R. Dahn, J. Electrochem. Soc. 144 (1997 2045).
[3] J.O. Besenhard, J. Yang, M. Winter, J. Power Sources 68 (1997) 87.
[4] J. Yang, M. Wachtler, M. Winter, J.O. Besenhard, Electrochem. Solid State Lett. 2 (1999) 161.
[5] M. Wachtler, J.O. Besenhard, M. Winter, J. Power Sources 94 (2001) 189.
[6] M. Wachtler, M. Winter, J.O. Besenhard, J. Power Sources 105 (2002) 151.
[7] K.D. Kepler, J.T. Vaughey, M.M. Thackeray, Electrochem. Solid State Lett. 2 (1999) 307.
[8] D. Larcher, L.Y. Beaulieu, D.D. Macneil, J.R. Dahn, J. Electrochem. Soc. 147 (2000) 1658.
[9] Y.Y. Xia., T. Sakai, T. Fujiedu, M. Wada, H. Yoshinaga, J. Electrochem. Soc. 148 (2001) A471.
[10] Y. Hamon, T. Brousse, F. Jousse, P. Topart, P. Buvat, D.M. Schleich, J. Power Sources 97–98 (2001) 185.
[11] R.Z. Hu, L. Zhang, X. Liu, M.Q. Zeng, M. Zhu, Electrochem. Commun. 10 (2008) 1109.
[12] R.A. Huggins, J. Power Sources 81–82 (1999) 13.
[13] A.J. Bard, L.R. Faulkner, Eelectrochemical Methods: Fundamentals and Applications, 2nd ed., John Wiley, 2000, p. 226.
[14] T. Zhang, L.J. Fu, J. Gao, Y.P. Wu, R. Holze, H.Q. Wu, J. Power Sources 174 (2007) 770.
[15] M. Winter, W.K. Appel, B. Evers, T. Hodal, K.C. Möller, I. Schneider, M. Wachtler, M.R. Wagner, G.H. Wrodning, J.O. Besenhard, Monatsh. Chem. 132 (2001) 473.